

Dynamical brittle fractures of nanocrystalline silicon using large-scale electronic structure calculations

Takeo Hoshi and Takeo Fujiwara

Department of Applied Physics, University of Tokyo, Bunkyo-ku, Tokyo 113-8656, Japan

(Dated: January 29, 2020)

A large-scale electronic structure method is developed and applied to nanocrystalline silicon with more than 10^5 atoms. Dynamical fracture processes are simulated under external loads in the [001] direction. In results, the fracture propagates anisotropically on the (001) plane and reconstructed surfaces appear with asymmetric dimers. Step structures are formed in larger systems, which are governed by the energy competition between short range quantum mechanical interaction and long range elastic interactions. Such energy competition may be a general foundation of nanostructures and can be described by the present total-energy method.

PACS numbers: 71.15.Pd, 62.20.Mk, 68.35.-p

Atomistic theories of nanocrystalline silicon are important for its mechanical properties, such as brittleness. A pioneering theory of brittle fracture was given, in 1920's, by Griffith¹ within a continuum theory, which is the foundation of the present understanding of macroscale brittle fractures^{2,3}. The key issue of the Griffith theory is the competition between the surface energy and the bulk (strain) energy. For the silicon case, the basic difference between the bulk and surface electronic states is the fact that the electronic wave functions in the bulk (diamond) structure are sp^3 -hybridized bonds but those in surface regions are not. *Ab initio* calculations can describe the above difference but consume large computational resources. Therefore, appropriate approximations are required for calculations of nanoscale systems with thousands of atoms or more. The present letter is devoted to such a practical method, based on two concepts of approximations; one is the total energy expressions with transferable sp tight-binding Hamiltonians, which can be used for several crystalline phases and non-crystalline phases, such as liquid⁴ and surfaces⁵. The other concept is the 'order-N' methods^{6,7,8}, in which the computational costs are linearly proportional to the system size.

One of the 'order-N' methods is given in the framework of the generalized Wannier states that are defined as unitary transformations of eigen states^{7,8,9,10,11}. The band structure energy is given as the sum of the one-electron energies of the occupied generalized Wannier states $\{\phi_i\}$;

$$E_{bs} = \sum_i^{\text{occ.}} \langle \phi_i | H | \phi_i \rangle. \quad (1)$$

The corresponding wave functions $\{\phi_i\}$ are localized and the index i denotes its localization center. We have proposed two order-N procedures, a variational one and a perturbative one, to obtain such localized wave functions⁸. The equation for wave functions is common between the two procedures but the perturbative procedure is simpler than the variational procedure.

With the combination of the above two procedures, we now construct a novel hybrid method, which is applicable to nanoscale systems of upto 10^5 atoms even without

parallel computation. Here the variational procedure is used for the wave functions near fracture regions. The regions contain, typically, 4×10^4 electrons. Some of such wave functions change their character dynamically from the bulk (sp^3 bonding) states to surface ones, as discussed later. The other wave functions, in bulk regions, keep the character of the bulk bonding state and can be obtained by the perturbative procedure. The total energy and any physical quantity are well defined in the above hybrid scheme, because they are expressed by the one-body density matrix ($\rho \equiv \sum_i^{\text{occ.}} |\phi_i\rangle\langle\phi_i|$).

To analyze the Wannier states in fracture processes, a parameter $f_s^{(j)}$ is defined, for a wave function ϕ_j , as

$$f_s^{(j)} \equiv \sum_I |\langle \phi_j | Is \rangle|^2, \quad (2)$$

where $|Is\rangle$ is the s orbital at the I -th atom. The values $f_s^{(j)}$ and $(1-f_s^{(j)})$ are the weights on the s and p orbitals, respectively. The parameter $f_s^{(j)}$ indicates the hybridization freedom of electronic states, whose dynamical change is crucial in the fracture processes. For the bulk Si case, our tight-binding calculation gives the value of $f_s = 0.36$, which deviates from the ideal sp^3 hybridization ($f_s = 1/4$). The physical origin of the deviation was systematically investigated among the group IV elements of the diamond structure (C, Si, Ge and α -Sn)⁸.

In this letter, we focus on the Si(001) surface, a standard template of the modern silicon technology. A characteristic feature in the Si(001) surface is the formation of asymmetric dimers^{12,13}. The asymmetric dimer is connected by a ' σ ' bonding state. Another state is localized on the 'up' atom, the dimerized atom near the vacuum region. This localized state is called ' π ' state, because the direction of its p components is nearly perpendicular to the dimer bond. Here an energy quantity is defined as

$$\Delta\varepsilon_i^{(\text{cov})} \equiv \langle \phi_i | H | \phi_i \rangle - \left[f_s^{(i)} \varepsilon_s + (1 - f_s^{(i)}) \varepsilon_p \right]. \quad (3)$$

A negative value of $\Delta\varepsilon_i^{(\text{cov})}$ corresponds to the energy gain of a covalent bonding. The ' σ ' state has the gain of

$\Delta\varepsilon_i^{(\text{cov})} \approx -2\text{eV}$, which mainly contributes to the dimerization energy (about -2eV)¹³. The ‘ π ’ state has much smaller $\Delta\varepsilon_i^{(\text{cov})}$, which is comparable to the energy difference between the asymmetric and symmetric dimers (the order of 0.1eV)¹³.

Hereafter, fractures of nanocrystalline silicon are simulated using a standard workstation with one CPU and 2 GB RAMs. The samples are isolated tetragonal clusters, whose geometries are labelled with the number of atomic layers in three axes, such as $n_{100} \times n_{010} \times n_{001}$ or $n_{110} \times n_{1\bar{1}0} \times n_{001}$. The Wannier states at the sample boundary surfaces are terminated by fixed sp^3 bonding states and are not reconstructed. The time step of the molecular dynamics is 3 fs. The atomic thermal motions are controlled to be 300 K by the Nose-Hoover thermostat method¹⁴. The numerical accuracy is checked in physical quantities important for fracture properties, such as the elastic constants, the asymmetric dimer on clean (001) surfaces and the critical stress for fracture. The last quantity is checked, with smaller samples, in comparison with the standard diagonalization method.

For fracture propagations, external loads in the [001] direction are imposed. In the initial states, the samples are prepared under deformations. During the simulations, the external loads can be dynamically controlled by the atoms on the sample boundaries in the z direction. These atoms are fixed or under artificial constant-velocity motions in the z axis. The velocity, typically the order of 0.01 km/s , is much smaller than that of observed fracture propagation velocities (in the order of km/s). As a seed of fractures, a short range repulsive potential is imposed on one particular pair of atoms, as a defect bond. When the fracture begins, the external loads are in the order of GPa, where the averaged bond length is about or less than 10 % longer than that in the ideal crystal. The averaged strain energy is in the order of 10^{-1} eV per bond, which is quite large but still smaller than that of the bond-breaking energy (the order of eV). We observe that if the samples do not contain the defect bond, the fracture do not occur with the above external load.

Figure 1(a) shows a typical elementary process during

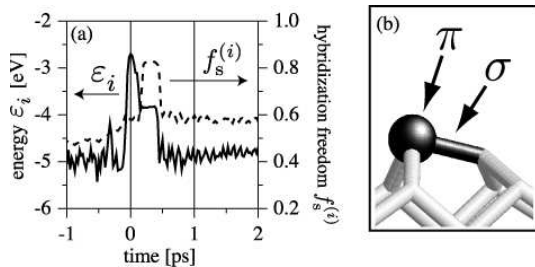


FIG. 1: (a) Elementary reconstruction process with the one-electron energy ε_i and the hybridization freedom, or the weight on s orbitals, $f_s^{(i)}$. (b) An asymmetric dimer on a resultant crack. The black rod and black ball correspond to the ‘ σ ’ and ‘ π ’ states, respectively.

successive bond breakings. We monitor the one-electron energy $\varepsilon_i \equiv \langle \phi_i | H | \phi_i \rangle$ and the hybridization freedom $f_s^{(i)}$ of a Wannier state $|\phi_i\rangle$. Before the bond breaking ($t < 0\text{ ps}$), the wave function $|\phi_i\rangle$ is a bonding state in the bulk region, deformed due to the external load. At $t \approx 0\text{ ps}$, a bond breaking occurs; the wave function $|\phi_i\rangle$ loses the bonding character with rapid increase of the bond length. Then ($0\text{ ps} < t < 0.2\text{ ps}$), a twofold coordinated surface atom appears, since another bond is broken almost simultaneously. The wave function $|\phi_i\rangle$ forms a metastable s-rich state with a high value of f_s , localized on an atom, not a bond. This s-rich atomic state is doubly occupied as a loan pair. The increase of $f_s^{(i)}$ ($0.6 \rightarrow 0.8$) causes the energy gain estimated to be $-0.2 \times (\varepsilon_p - \varepsilon_s) \approx -1.3\text{eV}$, which explains the energy gain in the figure ($\varepsilon_i = -2.7\text{eV} \rightarrow -3.8\text{eV}$). This energy gain stabilizes the unreconstructed surface atom. In other words, the bond breaking process is caused by the local electronic instability, that is, the energy competition between the *loss* of the bonding (transfer) energy and the *gain* due to the increase of the weight on the s orbitals (f_s). Finally, after the thermal motions with a finite time ($t \approx 0.4\text{ps}$), a pair of unreconstructed atoms forms an asymmetric dimer with a σ bonding state $|\phi_i\rangle$. The corresponding covalent-bonding energy, defined in Eq. (3), is $\Delta\varepsilon_i^{(\text{cov})} \approx -1.9\text{ eV}$. This energy explains the gain in the figure ($\varepsilon_i = -3.8\text{eV} \rightarrow -4.8\text{eV}$) and the energy *loss* (about 1.3eV) due to the decrease of $f_s^{(i)}$ ($0.8 \rightarrow 0.6$). This asymmetric dimer is preserved until the end of the simulation, during a couple of pico seconds. Figure 1(b) is an example of observed asymmetric dimers. The above two-stage reconstruction process is commonly observed in the present fracture simulations.

Figure 2 shows the fracture process of a cubic sample with 4501 atoms. Each Wannier state is classified from its weight distribution into a bonding or atomic orbital, which is shown as a rod or a ball in the figures, respectively. A *black* rod or ball corresponds to one in the layer that contains the defect bond. One almost flat (001) surface is being created with many asymmetric dimers¹⁵. The surface contains, however, many unreconstructed atoms that have two back bonds (white rods) and one doubly-occupied atomic orbital (black ball). This is because the unreconstructed atoms are metastable during thermally non-equilibrium dynamics within a few pico seconds. In Fig. 2, an anisotropic bond-breaking propagation is seen in the [110] and $[1\bar{1}0]$ directions, especially in the early snapshots. In the [110] direction, the successive bond breakings propagate along the *nearest neighbor* bond sites, which forms a zigzag path, as the black rods in Fig. 3(a). A bond breaking process drastically weakens the *nearest neighbor* bonds, due to the local electronic instability, observed in Fig. 1(a). Therefore, the successive bond breakings propagate easily in the [110] direction. In the $[1\bar{1}0]$ direction, on the other hand, the bond-breaking paths are not connected as the red rods in Fig. 3(a). In this direction, the bond break-

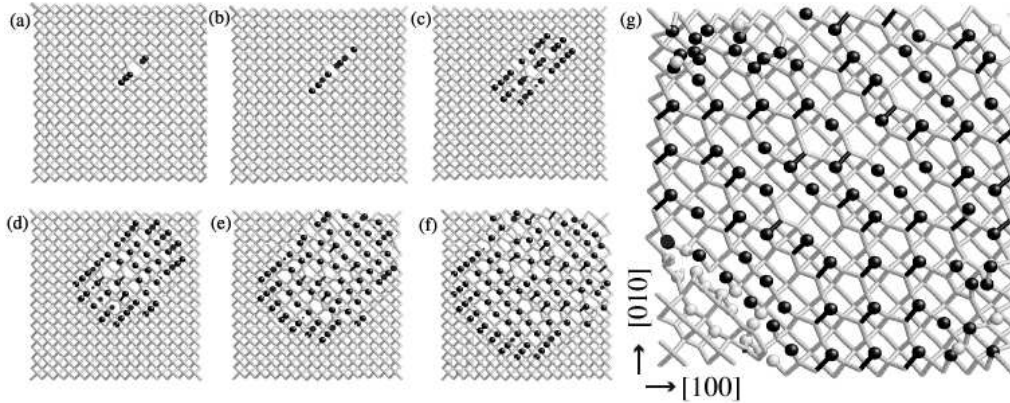


FIG. 2: Snapshots of a fracture process in the (001) plane. The sample size is $n_{100} \times n_{010} \times n_{001} = 33 \times 33 \times 33$ (4501 atoms). The time interval between two successive snapshots is 0.3 ps, except that between (f) and (g) (about 1.3 ps). A set of connected black rod and black ball corresponds to an asymmetric dimer, as in Fig. 1(b). The left-down area has not yet fractured.

ings are propagated through the local strain relaxation, not by the local electronic instability. In conclusion, the bond breaking propagation along the *nearest neighbor* bond sites (in the $[110]$ direction of the present surface) is faster than that in the perpendicular direction (in the $[1\bar{1}0]$ direction), due to the difference of the successive bond breaking mechanisms.

Figures 3 (b) and (c) show larger samples with step formations¹⁶. Between the two cases, all the conditions are the same, except the sample sizes. To see the step structures clearly, the broken bond sites are shown as rods in the *ideal* crystalline geometry. The defect bond is located in the center of the drawn area. If the anisotropy is ignored, the fracture propagation velocity can be estimated. For both cases, the velocity is in the same order of, but less than, the Rayleigh surface wave velocity (4.5km/s), as expected from the continuum theory².

The elastic property of silicon crystal shows only a small anisotropy within (001) plane; the $[110]$ and $[1\bar{1}0]$ directions are equivalent and the values of the Young modulus are different by only about 30 % in the $[100]$ and $[110]$ directions. The anisotropic bond-breaking propagation in one (001) plane increases the anisotropic strain energy. The anisotropy originates from the inequivalence between the $[110]$ and $[1\bar{1}0]$ directions within *one* (001) layer. Since the above inequivalence dose not appear within *two* successive layers, a step formation between them will release the anisotropic strain energy. In Fig. 3 (b), a step is formed between the layer of black rods and that of red rods. In the $[110]$ direction, the bond-breaking propagation reaches the sample boundaries without step formations. In the $[1\bar{1}0]$ directions, the bond-breakings propagate slower and a step is formed in the central area at an early period of the crack propagation. Here we observe that a step formation consumes an additional finite

time and so the bond-breaking propagation in the layer of *red* rods should start with a delay. We also observe that, during the delay time, the bond-breakings propagate in the layer of *black* rods both in the $[110]$ and $[1\bar{1}0]$ directions and so the resultant step formation path is almost a line in the $[100]$ or $[010]$ directions. In Fig.3(c), the largest sample in the present letter, the above line structure dose not reach the sample boundary but is terminated with additional step formations in complicated paths. If a sample contains many atoms that accumulate the strain energy, the geometry of the resultant crack will be almost circular with steps, as observed in Fig. 3 (c), so as to minimize the anisotropic strain energy. This is consistent to the fact that an atomistically flat (001) crack dose not grow in macroscale samples¹⁵.

In general, the atomistic picture for the brittle fracture of silicon is governed by the competition between short range quantum mechanical interactions and long range elastic interactions. In macroscale samples, a local fracture region, such as a crack tip, is under the long range elastic interactions with macroscopic regions^{2,3}. In nanoscale samples, due to the lack of the long range elastic interactions, mechanical properties are directly related by local quantum mechanical interactions and can be different from those in macroscale samples. Here a crossover can be expected among the sample sizes and may correspond to the presence or absence of step structures in the present calculations.

We present a novel hybrid method for large-scale electronic structure calculations with a well-defined total energy. The method can describe, as well as local surface reconstruction processes, the global energy competition between surface and bulk regions. Such energy competition governs the size and anisotropy of nano structures and may be a general foundations of nanoscale struc-

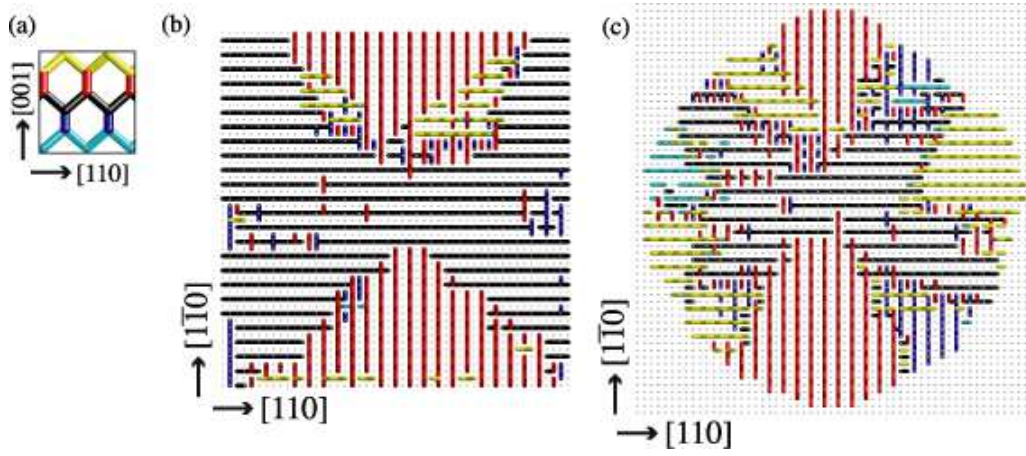


FIG. 3: (a) Ideal diamond structure with colored bond sites. (b)(c) Geometry of resultant cracks in the (001) plane. The broken bond sites are plotted as colored rods in the ideal (crystalline) geometry. Rods within one layer are painted in a same color, as in (a). The layer of black rods contains the defect bond at its central area. Atoms are plotted as dots. The sample sizes in (b) and (c) are $n_{110} \times n_{\bar{1}\bar{1}0} \times n_{001} = 49 \times 50 \times 49$ (30025 atoms) and $97 \times 100 \times 49$ (118850 atoms), respectively. In (c), only a central area ($n_{110} \times n_{\bar{1}\bar{1}0} = 58 \times 60$) of the sample is shown. Note that the length of $n_{110} = 50$ atomic layers is about 10 nm.

tural properties, for examples, brittle fracture, crystal growth, and self organization. The present letter implies the importance and applicability of large-scale electronic structure calculations for general nanoscale structures.

This work is supported by a Grant-in-Aid for COE Research ‘Spin-Charge-Photon’ and a Grant-in-Aid from

the Japan Ministry of Education, Science, Sports and Culture. This work is also supported by ‘Research and Development for Applying Advanced Computational Science and Technology’ of Japan Science and Technology Corporation.

- ¹ A. A. Griffith, Philos. Trans. R. Soc. London, Ser. A **221**, 163 (1920).
- ² As general references of brittle fracture, L. B. Freund, ‘Dynamic fracture mechanics’, Cambridge university press (1989); B. Lawn, ‘Fracture of brittle solids’, 2nd ed., Cambridge university press (1993).
- ³ For recent studies of the macroscale brittle fracture of Si, see the following papers and references therein; D. Holland and M. Marder, Phys. Rev. Lett. **80**, 746 (1998); R. Pérez and P. Gumbsch, Phys. Rev. Lett. **84**, 5347 (2000).
- ⁴ I. Kwon, R. Biswas, C. Z. Wang, K. M. Ho, and C. M. Soukoulis, Phys. Rev. B **49**, 7242 (1994).
- ⁵ For example, C.-C. Fu, M. Weissmann, A. Saúl, Surf. Sci. **494**, 119 (2001).
- ⁶ As reviews of the order-N methods, P. Ordejón, Comp. Mat. Sci. **12**, 157 (1998); S. Goedecker, Rev. Mod. Phys. **71**, 1085 (1999).
- ⁷ F. Mauri, G. Galli and R. Car, Phys. Rev. B **47**, 9973 (1993); P. Ordejón, D.A. Drabold, and M.P. Grumbach and R. M. Martin, Phys. Rev. B **48**, 14646 (1993).

- ⁸ T.Hoshi and T.Fujiwara, J. Phys. Soc. Jpn, **69**, No.12, 3773 (2000).
- ⁹ W.Kohn, Phys. Rev. B **7**, 4388 (1973).
- ¹⁰ W.Kohn, Chem. Phys. Lett. **208**, 167 (1993).
- ¹¹ N. Marzari and D. Vanderbilt, Phys. Rev. B **56**, 12847 (1997).
- ¹² D. J. Chadi, Phys. Rev. Lett. **43**, 43 (1979).
- ¹³ For an example of *ab initio* calculations, A Ramstad, G. Brocks, and P. J. Kelly, Phys. Rev. B **51**, 14504 (1995).
- ¹⁴ S. Nose, Mol. Phys. **52**, 255 (1984); W. G. Hoover, Phys. Rev. A **31**, 1695 (1985).
- ¹⁵ Unlike the present situations of nanoscale samples, macroscale samples has the (111) plane as the easiest cleavage plane. See Refs.^{2,3}.
- ¹⁶ The steps in the (001) surface are categorized in four types¹⁷. The present surfaces, however, contain many unreconstructed atoms and are different from the above ones.
- ¹⁷ D. J. Chadi, Phys. Rev. Lett. **59**, 1691 (1987).